Supplementary Information

Atomic-Scale Structure and Its Impact on Chemical Properties of Aluminum Oxide Layers Prepared by Atomic Layer Deposition on Silica

Monu Kaushik,[‡,a] César Leroy,[†,a] Zixuan Chen,[§] David Gajan,[‡] Elena Willinger,[§] Christoph R. Müller,[§] Franck Fayon,[†] Dominique Massiot,[†] Alexey Fedorov,[§] Christophe Copéret,[||] Anne Lesage,[‡,*] Pierre Florian[†,*]

[†] CNRS, CEMHTI UPR3079, Univ. Orléans, F-45071 Orléans, France

[‡] Centre de RMN à Très Hauts Champs, Université de Lyon (CNRS/ENS Lyon/UCB Lyon 1), 69100 Villeurbanne, France

[§] Department of Mechanical and Process Engineering, ETH Zürich, CH 8092 Zürich, Switzerland

[||]Department of Chemistry and Applied Biosciences, ETH Zürich, CH 8093 Zürich, Switzerland

[a] These authors contributed equally

* Corresponding author : Anne Lesage (anne.lesage@ens-lyon.fr),

Pierre Florian (pierre.florian@cnrs-orleans.fr)

Characterization techniques

Diffuse reflectance infrared Fourier transform spectroscopy (DRIFTS) was performed on an Alpha II spectrometer (Bruker) operated inside an MBraun glovebox (O_2, H_2O < 1 ppm). Atomic layer deposition of trimethylaluminum (TMA, Pegasus Chemicals) onto SiO_{2-500} using ozone as an oxidant was performed on a Picosun R-200 system enclosed within an MBraun glovebox (O_2, H_2O < 1 ppm). N_2 (99.999%) was used as the carrier and purge gas in the ALD experiments. The ozone concentration expected at the power used is 10% w/w (140 g Nm^{-3}). Elemental analysis was performed by the Mikroanalytisches Labor Pascher, Remagen, Germany. Transmission electron microscopy (TEM), scanning transmission electron microscopy (STEM) with high-angle annular dark-field (HAADF) detection, and energy-dispersive X-ray (EDX) spectroscopy were carried out on an FEI Talos F200X transmission electron microscope. A JEOL JEM-ARM300F Grand ARM scanning transmission electron microscope that was operated at 300 kV was also used. The microscope is equipped with a Dual EDS system (two large area SDD EDX detectors with 100 mm^2 active area; total solid angle: 1.6 sr). The specimen for electron microscopy were prepared by dry deposition onto a copper grid with a holey carbon support film. Where indicated, the vacuum-transfer holder (Mel-Build) has been used. The surface area and pore volume of the materials were determined by N_2 adsorption/desorption (Quantachrome NOVA 4000e) using the Brunauer-Emmet-Teller (BET) and Barrett-Joyner-Halenda (BJH) models, respectively.[1] Prior to the measurement, the materials were outgassed at 250 °C for 2.5 hours. Powder X-ray diffraction (XRD) data were collected on a PANalytical Empyrean X-ray diffractometer equipped with a Bragg-Brentano HD mirror and operated at 45 kV and 40 mA using Cu Kα radiation (λ = 1.5418 Å). The materials were examined within the 2ϑ range of 5-100° using a step size of 0.0167°. The scan time per step was 5 s.

Materials

Silica powder (AdValue Technology, 99.9%) was agglomerated into larger particles by wetting with water that was then evaporated slowly at 120 °C (2 days). Silica agglomerates were sieved to collect a 180-300 μm fraction. The sieved support was heated (5 °C min^{-1}) to and held overnight at 500 °C in static air, and then dehydroxylated at 500 °C (ca. 10^{-5} mbar, 20 h). The resulting material, denoted SiO_{2-500}, had a surface area of 374 m^2 g^{-1} and a pore volume of 2.0 ml g^{-1} according to N_2 physisorption measurements.

1, 5 or 10 ALD cycles were performed at 300 °C to deposit TMA onto SiO_{2-500} (300 mg). One ALD cycle includes, consecutively, 30 TMA pulses (0.4 s duration) and 20 ozone pulses (0.4 s duration). Each TMA or ozone pulse was followed by a N_2 purge (15 s duration). The temperature of the TMA source was 20 °C. As-prepared materials (TMA1-SiO_{2-500}, TMA5-SiO_{2-500} and TMA10-SiO_{2-500}) were calcined in synthetic air (500 °C, 5 °C min^{-1}, 50 ml min^{-1}, 4 h), which gave Al1−SiO_{2-500}, Al5−SiO_{2-500}, Al10−SiO_{2-500}.

^{15}N-Pyridine (99% isotopic enrichment) was purchased from CortecNet Corp., dried over CaH_2 at 60 °C overnight and degassed prior to use. Adsorption of pyridine on the calcined materials (ca. 100 mg) was performed in a glass reactor by exposing Al−SiO_{2-500} to ^{15}N-pyridine vapor at room temperature for ca. 1 min. The excess of ^{15}N-pyridine was then removed at high vacuum at 150 °C (ca. 10^{-5} mbar, 2 h). All materials were prepared, stored, handled and characterized without exposure to air, using N_2-filled gloveboxes (MBraun, O_2, H_2O < 1 ppm).

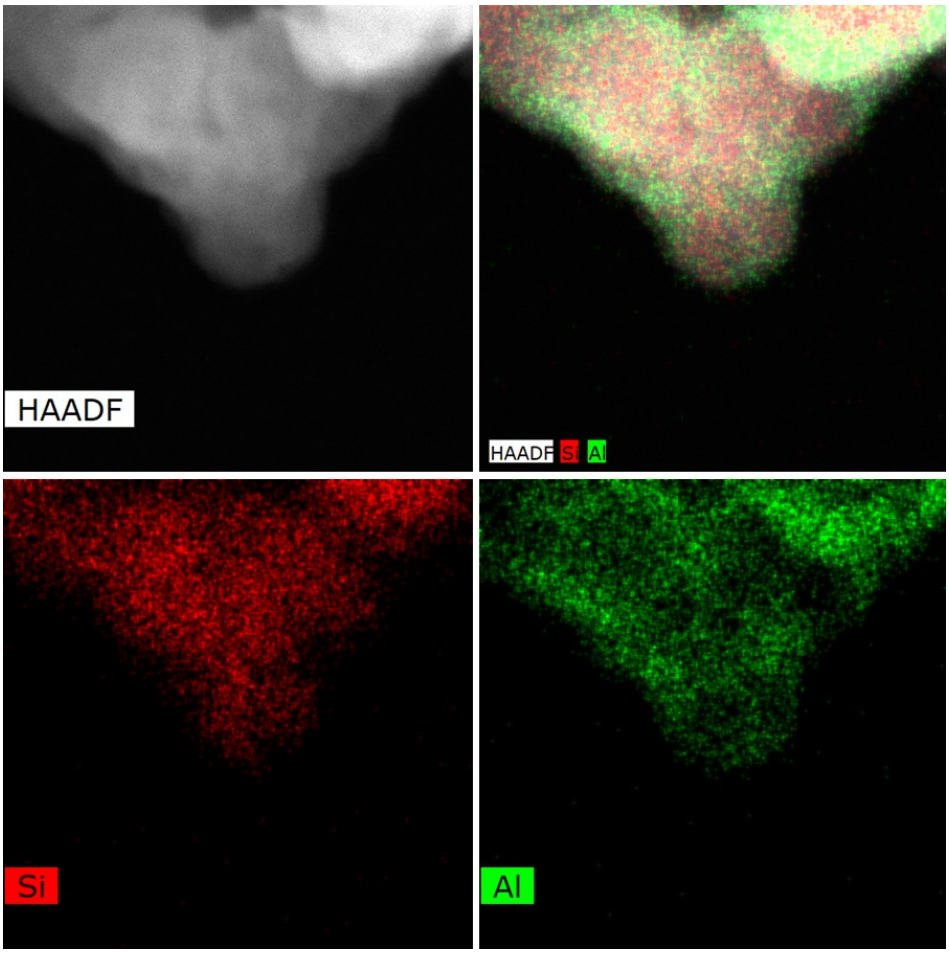

Figure S1. HAADF-EDX imaging of Al10−SiO_{2-500}, which was chosen as a representative material for the Al−SiO_{2-500} series.

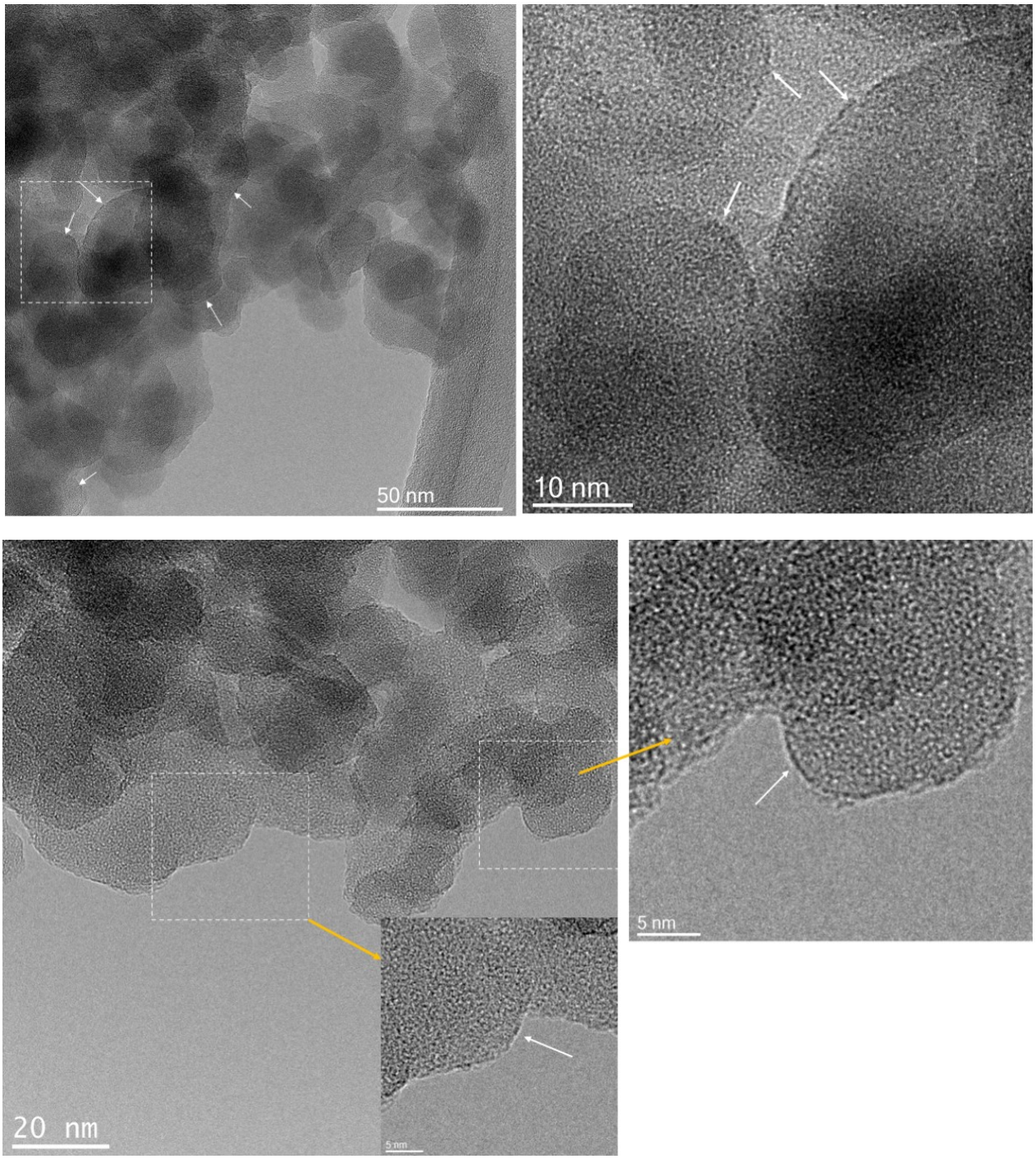

Figure S2. Representative images of a control HRTEM experiment in which Al5−SiO_{2-500} was handled using an air-tight TEM sample transfer holder. White arrows indicate ALD-grown coatings.

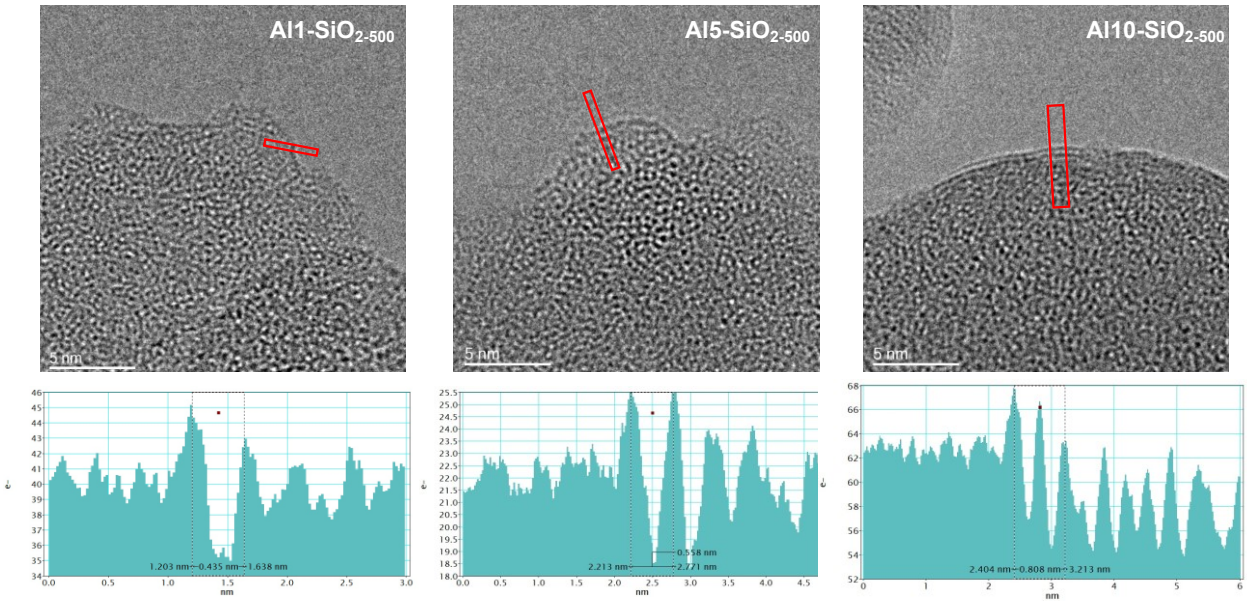

Figure S3. Intensity profiles for the ALD-derived alumina layers in Al1−, Al5− and Al10−$SiO_{2\text{-}500}$ materials. Scale bar: 5 nm.

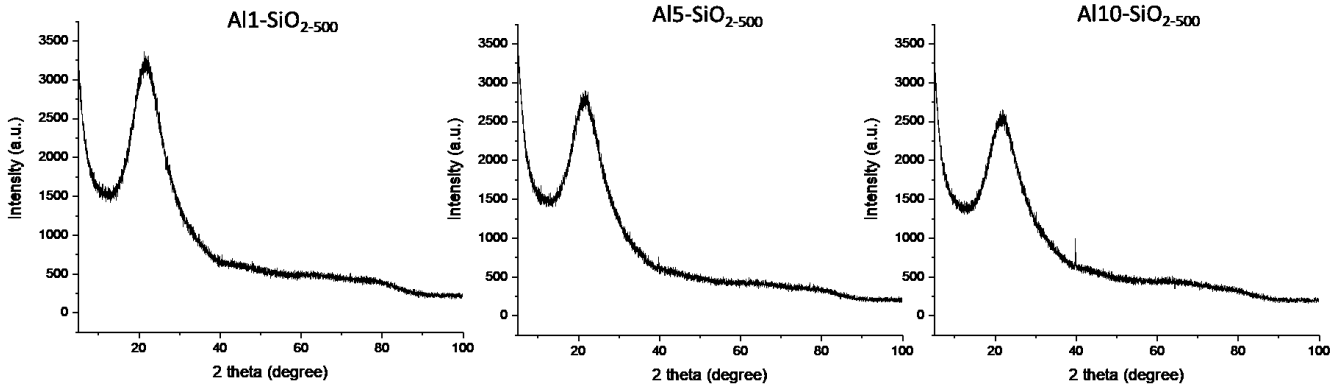

Figure S4. XRD patterns of Al1−, Al5− and Al10−$SiO_{2\text{-}500}$ materials.

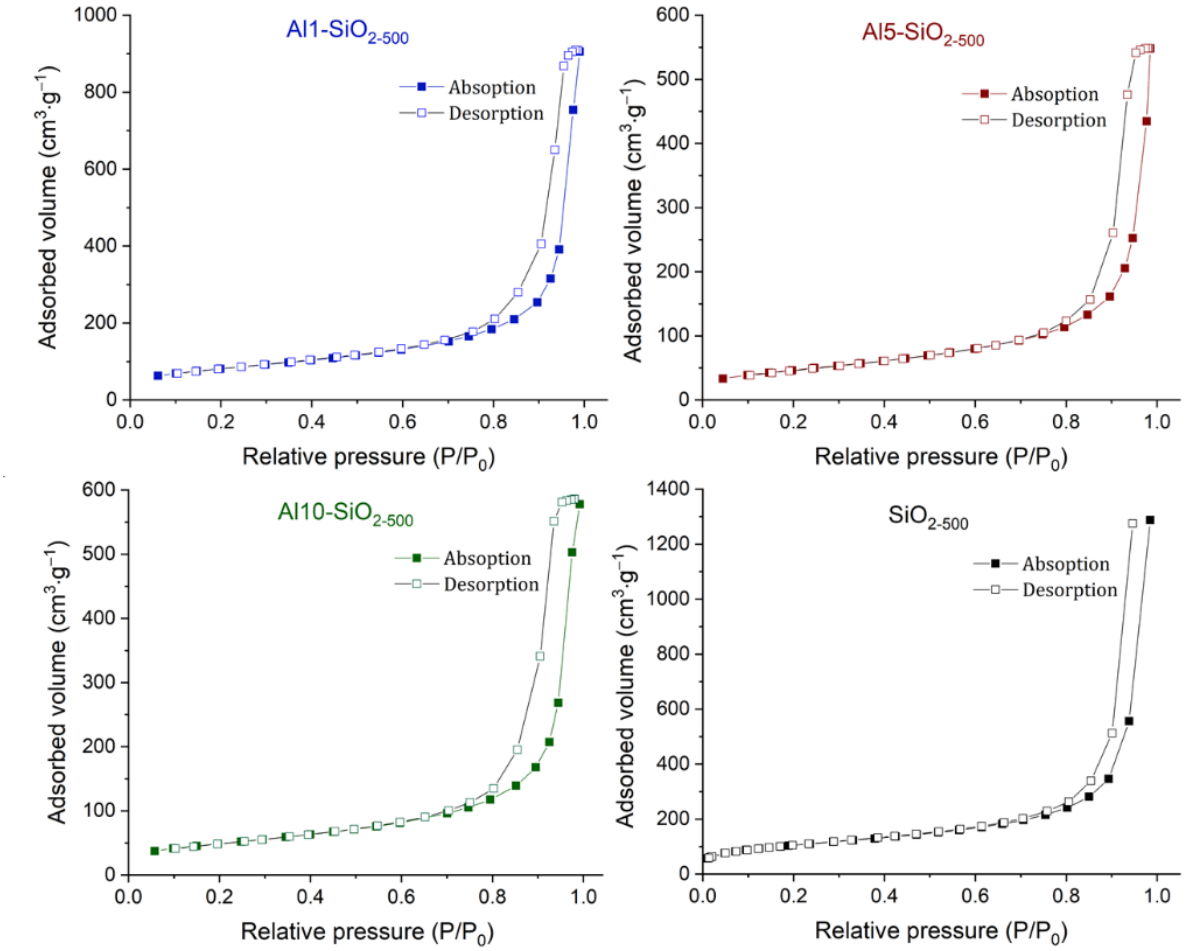

Figure S5. N_2 adsorption and desorption isotherms of Al1−, Al5− and Al10−SiO_{2-500} and SiO_{2-500} materials.

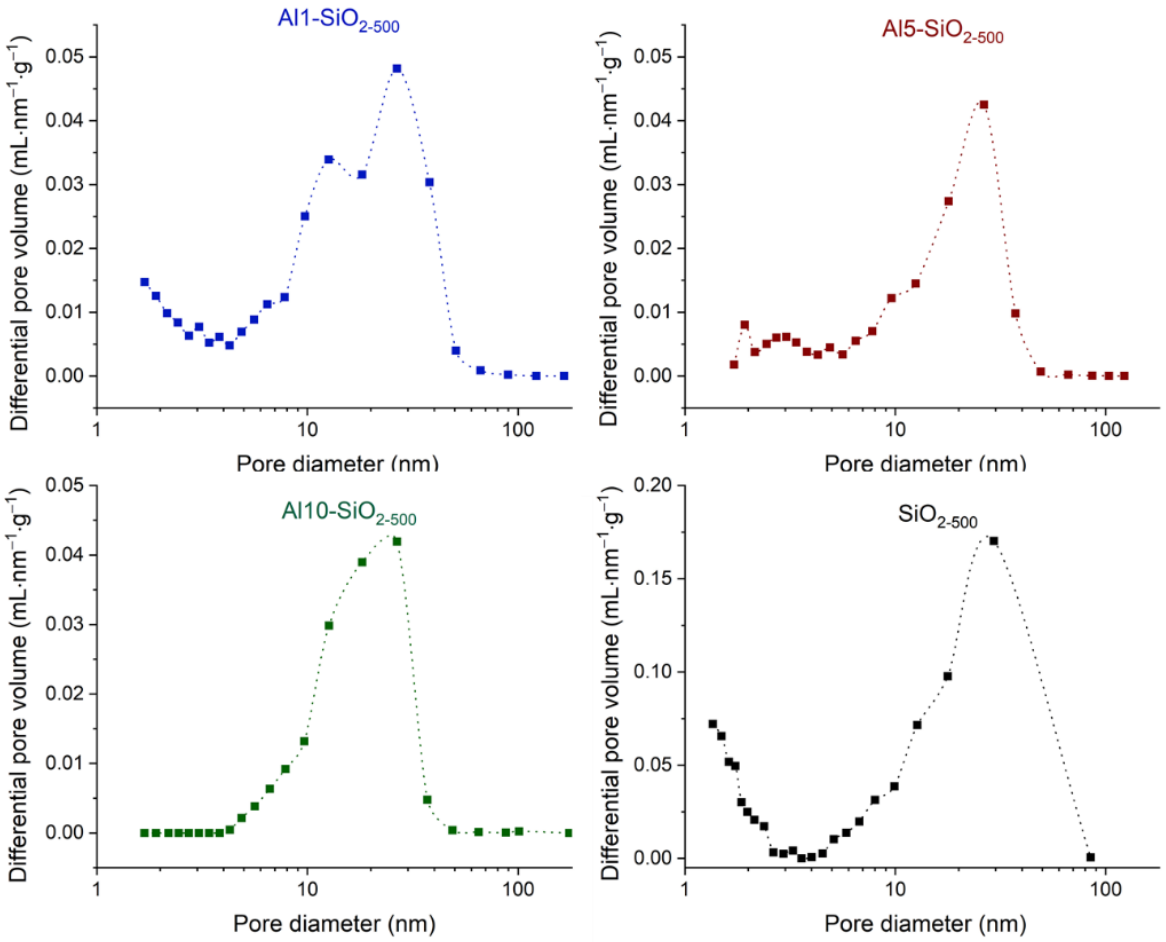

Figure S6. BJH pore size distribution of Al1−, Al5− and Al10−SiO_{2-500}, and SiO_{2-500} materials obtained from N_2 isotherms (Figure S5).

Table S1. BET surface area, pore volume and pore diameter for SiO_{2-500} and Al1−, Al5− and Al10−SiO_{2-500} materials.

Materials	BET surface area ($m^2\ g^{-1}$)	Pore volume ($cm^3\ g^{-1}$)	Pore diameter (nm)
SiO_{2-500}	374	2.0	29.4
Al1−SiO_{2-500}	287	1.4	26.6
Al5−SiO_{2-500}	168	0.9	26.4
Al10−SiO_{2-500}	173	0.9	26.6

Appearance of crystalline areas. On Al5− and Al10−SiO_{2-500}, areas can be found where few crystalline planes form a zigzag coating on a silica surface (Figure 1f and Figure S2). That being said, the zigzag coating does not appear on every silica grain, and a smooth coating (i.e. a coating following the curvature of silica grains) is a more abundant morphology of the ALD-deposited coatings. Consistent with the TEM analysis, the observed nanocrystalline zigzag pattern does not provide XRD peaks, as all three prepared Al−SiO_{2-500} materials are amorphous by XRD (Figure S4). However, a careful survey of selected area electron diffraction (SAED) data of Al10−SiO_{2-500} material reveals that, although rarely, this local method can resolve one set of planes corresponding to a d-spacing of ca. 1.96 Å ± 0.05 Å (inset, Figure 1f). This value of d_{hkl} corresponds to the most intense reflection expected for corundum α-Al_2O_3 ($d_{-2,2,2}$ = 1.9641 Å) but also to a significant reflection of transition alumina γ-Al_2O_3 ($d_{0,0,4}$ = 1.9677 Å) and kyanite $Al_2Si_2O_5$ ($d_{-1,4,0}$ = 1.9630, although this compound is expected to form at high pressure). It can also be found in gibbsite $Al(OH)_3$ and other $Al_2Si_2O_5$ polymorphs (andalusite and sillimanite), however, with very small intensities. Although a form of alumina seems to be a reasonable candidate, with only one measured d_{hkl} value (other observed crystalline zones were too small to provide electron diffraction), this cannot be confirmed.

In a control HRTEM experiment, Al5−SiO_{2-500} was evaluated using an air-tight TEM sample transfer holder, i.e. without exposing this material to air (Figure S2). Images of the surface layer obtained were not distinguishable from that in Figure 1e. This result confirms that the Al-containing coating layer does not restructure or crystallize during the time scale of a TEM experiment upon exposure to ambient air during specimen handling. Interestingly, the post-deposition crystallization of Al_2O_3 films with thicknesses comparable to that found in Al5− and Al10−SiO_{2-500} materials requires high temperatures (ca. 900 °C), which exceed significantly the calcination temperature used in this work (500 °C).[2] This suggests that the nanocrystalline zigzag structures likely have formed already in the as-deposited TMA5-SiO_{2-500} and TMA10-SiO_{2-500}. Yet the deposition of crystalline Al_2O_3 coatings is typical for high temperature ALD recipes (above 600 °C) that use $AlCl_3$ precursor.[2] Thus, formation of nanocrystalline zigzag structures observed in this work in Al5− and Al10−SiO_{2-500} materials, prepared at relatively low temperatures, is unexpected and likely due to the use of dehydroxylated silica.

NMR Room Temperature Spectroscopy. Direct excitation Hahn echo ^{27}Al NMR spectra were acquired using an Avance III standard bore 23.5 T Bruker spectrometer. All samples were packed in a 2.5 mm zirconia rotor inside an argon-filled glovebox. The rotor was spun at 33.3 kHz under pure nitrogen gas. ^{27}Al chemical shift is referenced to a nitric 1M solution of $Al(NO_3)_3$ while ^{1}H and ^{29}Si positions are referenced to tetramethylsilane. Double-frequency sweep (DFS) has been used in all experiments with ^{27}Al detection, except for the quantitative 1 pulse, with a 1 ms double sweep ranging from 1 MHz down to 200 kHz and a radio-frequency amplitude of 40 kHz.

Table S2. Details of the experimental parameters used for room-temperature NMR studies in this work.

Exp^{t}	nuclei	Field (T)	$\emptyset_{rotor}$ (mm)	ν_r (kHz)	rcycl (s)	# scans (x 1000)	# echos / τ (ms)	ν_{rf} (kHz)	pulses (µs)	Δt_1 (µs)	# t_1
1 pulse	^{27}Al	20.0	2.5	33.3	0.05	65 – 430		50	0.5		
Hahn echo	^{27}Al	20.0	2.5	33.3	0.5	8		50	1.67		
MQMAS	^{27}Al	20.0	2.5	33.3	0.5	2 – 8		140 / 25	3.5,1.25 / 4.17	30.0	24
CPMG	^{29}Si	9.4	4.0	10.0	900	0.1	512 / 8.0	28.6	8.75,17.5		
CP-CPMG	^{29}Si	9.4	4.0	10.0	1.0	2	512 / 8.0	28.6	8.75,17.5 / 500		
	^{1}H							50.0	5.0	200	24
D-HMQC	^{27}Al	20.0	2.5	30.0	1.0	2 – 6		50	1.67		
	^{1}H							130 / 60	1.95 /400	33.3	32
D-HMQC	^{27}Al	20.0	3.2	15.0	0.5	10 – 15		20	4.17		
	^{29}Si							26 / 30	9.5 / 6400	33.3	22
DQ/SQ	^{27}Al	20.0	2.5	33.3	0.3	11 – 70		20 / 16.7	4.2 / 480	30.0	20

DNP NMR at 9.4 T and 18.8 T. DNP experiments were performed at CRMN Lyon on Bruker Avance III wide bore spectrometers, operating at 9.4 T and 18.8 T, and equipped with triple resonance 1.3 mm and 3.2 mm low-temperature MAS probes in either H/C/N or H/Al/Si configuration. Cross-effect DNP was achieved by irradiation with high-power microwaves at frequencies of 263 GHz (for 9.4 T) and 527 GHz (for 18.8 T) generated by gyrotrons operating continuously during the DNP experiments (stability higher than ±1%). A microwave power of 40 W was used at 9.4 T, and 22 W at 18.8 T, both measured at the bottom of the probe. A triple-resonance probe in H/C/N configuration was used. The ^{27}Al chemical shifts are referenced to 0 ppm for a solution of $Al(NO_3)_3$ in HNO_3, ^{29}Si chemical shifts are referenced to tetramethylsilane, while ^{15}N chemical shifts are referenced externally by calibrating the chemical shift of NH_4Cl to 59.3 ppm with respect to NH_3.

Py-Al−SiO_{2-500} series. The materials were packed in an argon-filled glove box, with tetrachlororethane (TCE) as the impregnating solvent with either 16 mM TEKPol (for 9.4 T) or 16 mM HyTEK2 (for 18.8 T) radical. Once removed from the glove box, the packed rotor was immediately inserted into a low-temperature DNP probe pre-cooled to 105 K. For the ^{27}Al experiments, the 1.3 mm rotor was spun at the maximum spinning rate of 39 or 40 kHz. DR-INEPT (with $SR4_1^2$ recoupling) and CP experiments were optimized on impregnated γ-Al_2O_3 under the same conditions. Enhancements and DNP buildup times were recorded for each sample. ^{1}H-^{15}N CP experiments were performed with a spinning rate of 12 kHz and a contact time of 4 ms.

^{29}Si DNP NMR. Al−SiO_{2-500} samples were impregnated with a 16 mM TEKPol solution in TCE. Under DNP conditions, i.e. when the samples are exposed to microwave irradiation at 100 K, polarization transfer takes place. First, hyperpolarized unpaired electrons in the radical spread polarization to adjacent nuclei such as abundant protons. This enhanced polarization is transferred to ^{29}Si by CP, which is possible by direct ^{1}H to ^{29}Si transfer if the solvent and silica core are in contact. This is probably true for Al1−SiO_{2-500}. After 5 and 10 ALD cycles, a layer of aluminum oxide is present between the polarizing solvent and the silica core. The fact that enhanced polarization is still transferred to ^{29}Si in Al10−SiO_{2-500} suggests that the

polarization is relayed through the aluminum oxide layer by the proton network assisted spin-diffusion. A signal enhancement of > 20 is observed for all samples via ^{1}H-^{29}Si CP. If protons were localized in the vicinity of ^{29}Si, the intensity of the CP signal would remain unchanged upon microwave irradiation.

^{27}Al DNP NMR. The surfaces of materials onto which pyridine adsorbed contain ^{27}Al sites as well as the ^{15}N probe nuclei from the adsorbed ^{15}N-labelled pyridine. Both of these species can be detected by using appropriate proton to X nuclei polarization transfer pulse sequences. DNP samples were prepared by incipient wetness impregnation with the best performing radicals at each field, i.e., 16 mM TEKPol for 9.4 T, and HyTEK2 for 18.8 T in TCE. DNP enhanced ^{27}Al NMR spectra were also recorded at a high magnetic field. An INEPT-based transfer was implemented, as it has been recently shown to provide an enhanced sensitivity over CP transfer without causing lineshape distortions.[3] Moreover, ^{27}Al spectra were recorded at a higher magnetic field using both pulse sequences to obtain a better resolution. However, due to broad quadrupolar interaction and its anisotropic nature, it is not possible to resolve each ^{27}Al site even at 18.8 T.

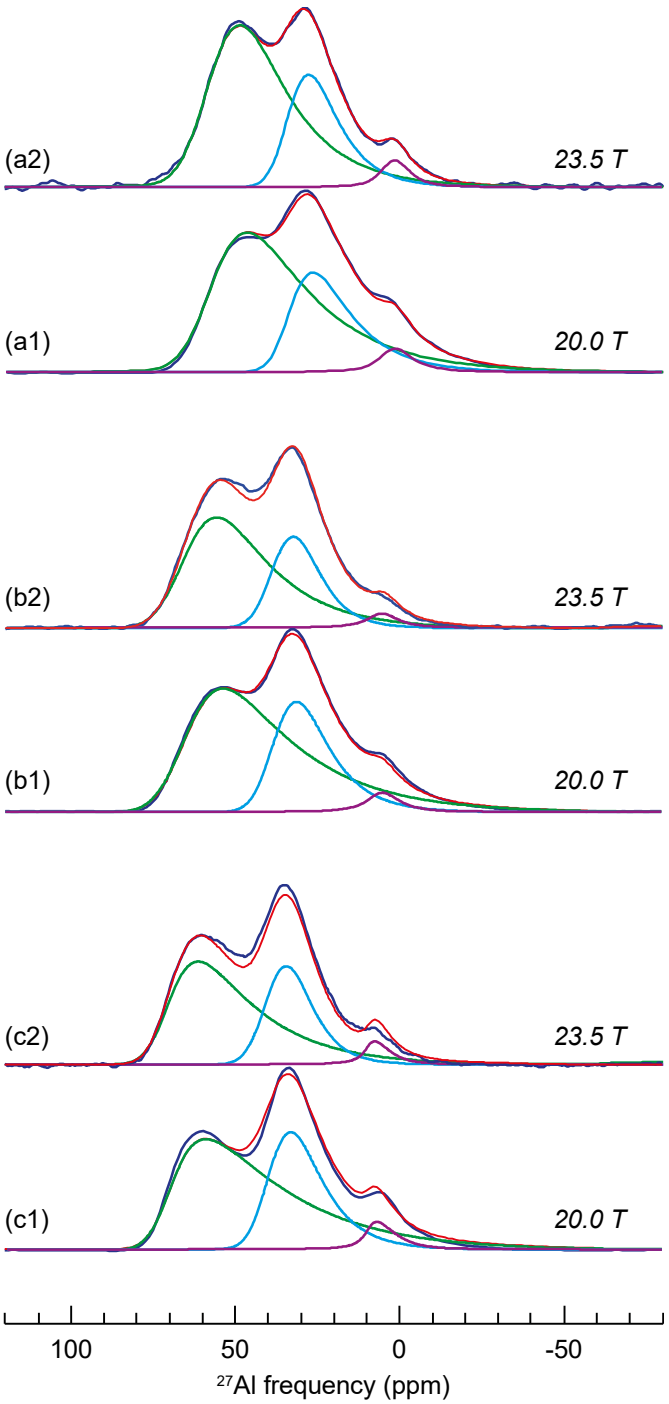

Figure S7. 1D ^{27}Al full Hahn-Echo experiments performed at 20.0 T and 23.5 T on (a) Al10−SiO_{2-500}, (b) Al5−SiO_{2-500} and (c) Al1−SiO_{2-500}. Experiments are displayed in blue, simulation in red and the individual components for $^{[4]}$Al, $^{[5]}$A, and $^{[6]}$Al sites are in green, blue and purple, respectively. Simulations are performed simultaneously on both fields assuming three GIM components.

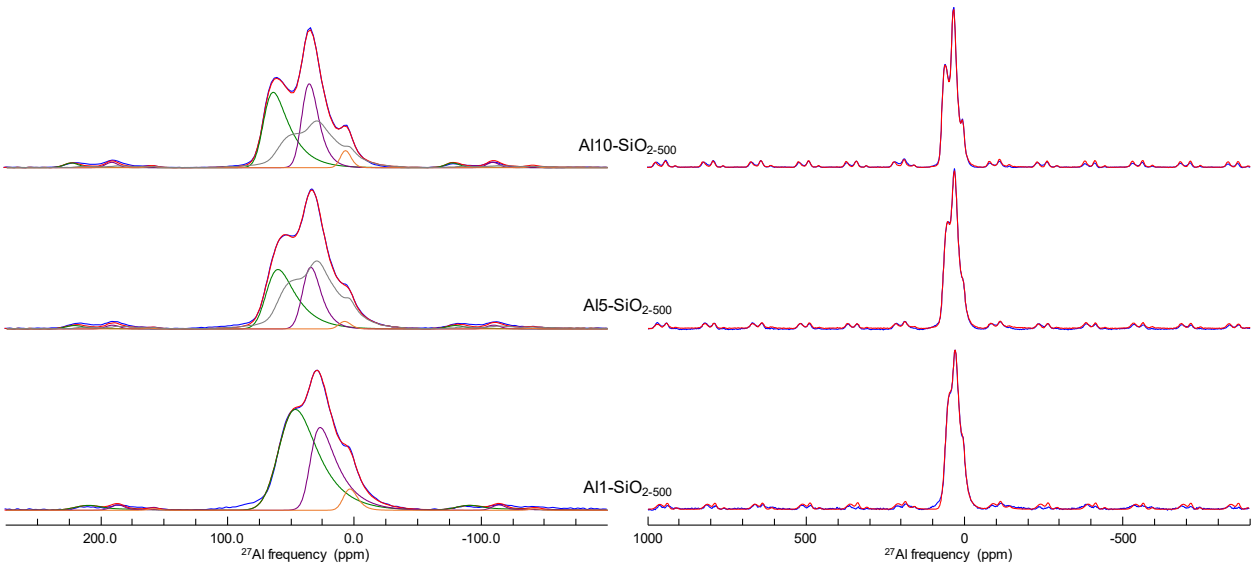

Figure S8. 1D ^{27}Al quantitative one-pulse MAS experiments performed at 20.0 T on Al10−SiO_{2-500} (top), Al5−SiO_{2-500} (middle) and Al1−SiO_{2-500} (bottom). Experiments are displayed in blue, simulation in red and the individual components for $^{[4]}$Al, $^{[5]}$Al and $^{[6]}$Al (orange) sites are in green, purple and orange respectively. The additional grey line is the experimental spectra of Al1−SiO_{2-500} used as a fourth component in the simulation.

Table S3. NMR parameters derived from the simulation of the quantitative one-pulse and Hahn echo experiments at 20.0 T. For Al1-SiO_{2-500}, the Hahn Echo spectrum simulation is performed simultaneously at 20.0 T and 23.5 T.

	Quantitative 1 pulse					Hahn Echo				
site	%	$\bar{\delta}_{iso}$ (ppm)	$\Delta\delta_{iso}$ (ppm)	$\Delta\nu_{1/2}$ (kHz)	$\bar{C}_Q$ (MHz)	%	$\bar{\delta}_{iso}$ (ppm)	$\Delta\delta_{iso}$ (ppm)	$\Delta\nu_{1/2}$ (kHz)	$\bar{C}_Q$ (MHz)
Al1−SiO_{2-500}										
$^{[4]}$Al	60	58.9	22.5		12.0	67	58.7	16.3		12.7
$^{[5]}$Al	35	35.3	10.9		10.9	29	34.1	11.2		10.0
$^{[6]}$Al	5	7.3	9.9		6.21	4	2.5	6.50	5.37	4.08
Al5−SiO_{2-500}										
$^{[4]}$Al	29	69.7	14.6		11.0	27	69.4	12.0		10.9
$^{[5]}$Al	19	39.9	11.8		7.67	17	39.1	10.2		7.85
$^{[6]}$Al	1	10.2	9.4		4.84	2	9.5	8.2		5.34
Al1	51					54				
Al10−SiO_{2-500}										
$^{[4]}$Al	35	72.1	11.8		10.5	31	71.2	11.5		9.38
$^{[5]}$Al	25	40.6	10.8		7.39	23	40.0	9.8		7.47
$^{[6]}$Al	3	9.7	8.12		4.97	4	9.6	8.0		5.57
Al1	37					43				

Table S4. Calculated errors of the NMR parameters, derived by DMFit during the fitting procedure.

	Quantitative 1 pulse					Hahn Echo				
site	%	$\bar{\delta}_{iso}$ (ppm)	$\Delta\delta_{iso}$ (ppm)	$\Delta\nu_{1/2}$ (kHz)	$\bar{C}_Q$ (MHz)	%	$\bar{\delta}_{iso}$ (ppm)	$\Delta\delta_{iso}$ (ppm)	$\Delta\nu_{1/2}$ (kHz)	$\bar{C}_Q$ (MHz)
Al1−SiO_{2-500}										
$^{[4]}$Al		0.4	0.11		0.40	1.0	0.13	0.23		0.13
$^{[5]}$Al		0.2	0.09		0.24	5.1	0.06	0.23		0.07
$^{[6]}$Al		0.5	0.20		0.48	1.8	0.22	0.88	17.0	0.28
Al5−SiO_{2-500}										
$^{[4]}$Al		0.2	0.07		0.33	0.6	0.09		0.18	0.10
$^{[5]}$Al		0.1	0.06		0.16	0.4	0.11		0.21	0.10
$^{[6]}$Al		0.9	0.29		0.95	0.2	0.39		0.58	0.37
Al1										
Al10−SiO_{2-500}										
$^{[4]}$Al		0.2	0.07		0.26	1.4	0.18		0.42	0.22
$^{[5]}$Al		0.1	0.05		0.17	0.7	0.22		0.39	0.19
$^{[6]}$Al		0.5	0.17		0.58	0.6	0.53		1.31	0.48
Al1										

Table S5. NMR parameters derived from the simulation of the two-dimensional ^{27}Al 3QMAS experiments performed on Al10−SiO_{2-500} (at 20.0 T and 23.5 T), Al5−SiO_{2-500} and Al1−SiO_{2-500}.

site	%	$\bar{\delta}_{iso}$ (ppm)	$\Delta\delta_{iso}$ (ppm)	$\bar{C}_Q$ (MHz)	%	$\bar{\delta}_{iso}$ (ppm)	$\Delta\delta_{iso}$ (ppm)	$\bar{C}_Q$ (MHz)
	20.0 T				23.5 T			
Al1−SiO_{2-500}								
$^{[4]}$Al	56	61.8	11.1	11.65				
$^{[5]}$Al	36	33.5	10.7	7.07				
$^{[6]}$Al	8	4.8	5.6	5.59				
Al5−SiO_{2-500}								
$^{[4]}$Al	47	67.2	11.9	9.4				
$^{[5]}$Al	46	37.2	9.6	7.3				
$^{[6]}$Al	8	6.5	8.6	4.5				
Al10−SiO_{2-500}								
$^{[4]}$Al	42	70.7	13.7	8.4	45	69.4	12.6	8.2
$^{[5]}$Al	48	39.6	10.7	7.2	48	39.8	11.9	7.5
$^{[6]}$Al	10	8.0	9.6	4.6	7	9.0	9.9	5.7

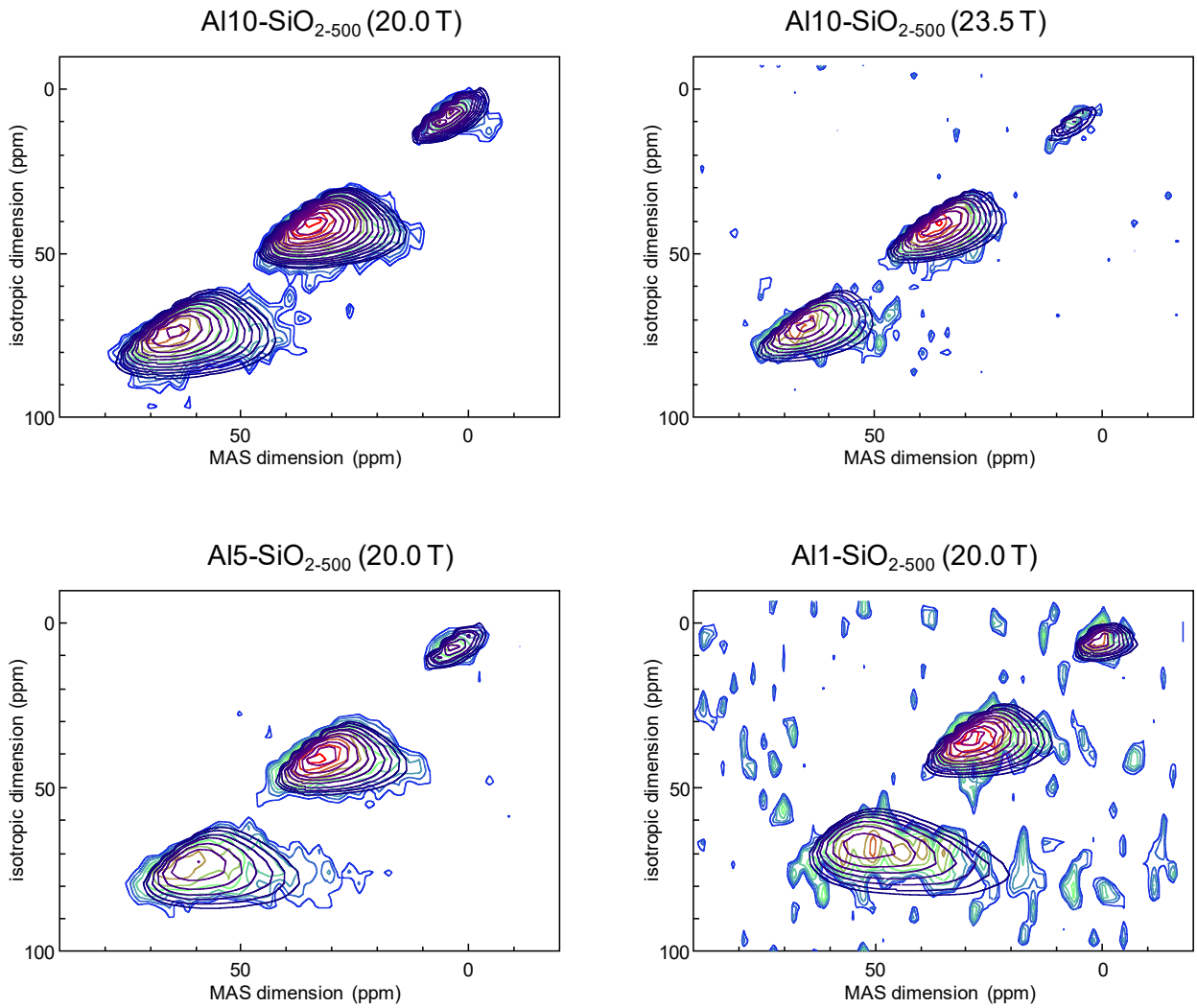

Figure S9. 2D ^{27}Al 3QMAS experiments performed on Al10−SiO_{2-500} at 20.0 T (top left) and 23.5 T (top right), Al5−SiO_{2-500} (bottom left) and Al1−SiO_{2-500} (bottom right). Experiments are displayed in color and GIM model-based simulations are displayed in purple.

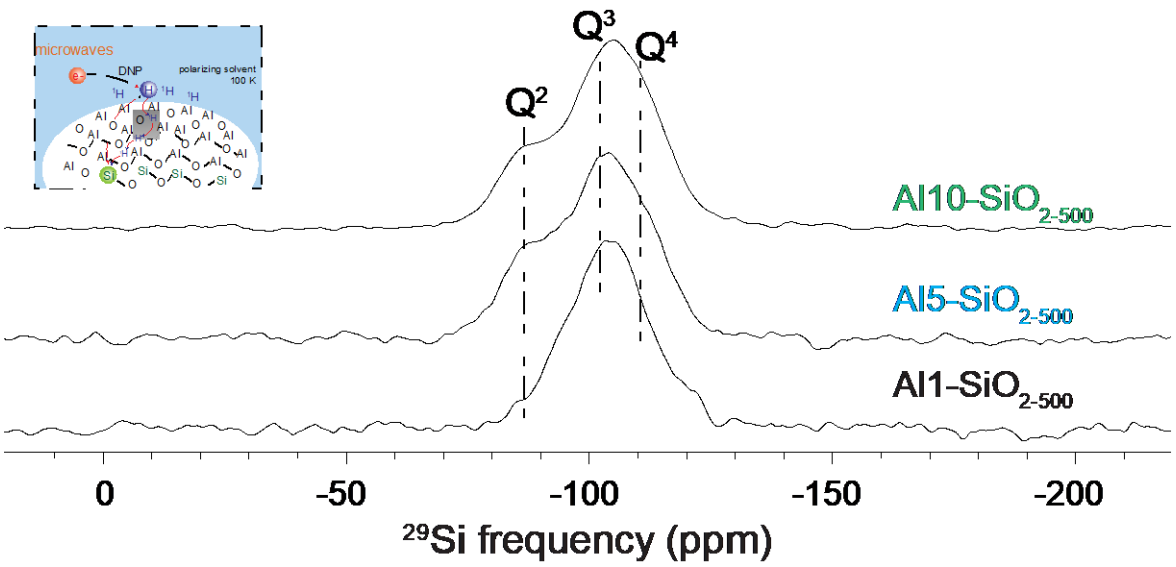

Figure S10. DNP enhanced $^{29}Si\{^{1}H\}$ CP experiment on Al1−SiO_{2-500} (black), Al5−SiO_{2-500} (blue), and Al10−SiO_{2-500} (green) measured at 9.4 T with a 3.2 mm triple resonance probe. In the experiments, 10 kHz MAS and a sample temperature of 100 K were employed along with irradiating microwaves of power 40 W. The expected chemical shifts of Q^2, Q^3, and Q^4 sites are represented by vertical dotted lines. The schematic in the inset shows a simplified sketch of the DNP process.

Table S6. ^{27}Al and ^{1}H calculated errors of the NMR parameters derived from the simulation of the 2D $^{27}Al\{^{1}H\}$ D-HMQC experiment performed on Al1−SiO_{2-500} and Al10−SiO_{2-500}.

site	%	$\bar{\delta}_{iso}$ (ppm)	$\Delta\delta_{iso}$ (ppm)	$\bar{C}_Q$ (MHz)
Al1−SiO_{2-500}				
$^{[4]}Al$		0.05	0.24	0.06
$^{[5]}Al$		0.07	0.06	0.07
$^{[6]}Al$		0.11	0.67	0.02
$H_{(1)}$		0.03	0.03	
$H_{(2)}$		0.01	0.02	
Al10−SiO_{2-500}				
$^{[4]}Al_{extra}$		0.11	0.51	0.15
$^{[4]}Al$		0.05	0.21	0.05
$^{[5]}Al$		0.02	0.03	0.03
$^{[6]}Al$		0.07	1.02	0.13
H-$^{[4]}Al_{extra}$		0.07	0.18	
$H_{(1)}$-$^{[4]}Al$		0.36	0.43	
$H_{(2)}$-$^{[4]}Al$		0.13	0.43	
$H_{(1)}$-$^{[5]}Al$		0.42	0.38	
$H_{(2)}$-$^{[5]}Al$		0.07	0.25	
$H_{(1)}$-$^{[6]}Al$		0.31	0.38	
$H_{(2)}$-$^{[6]}Al$		0.09	0.32	

Table S7. ^{27}Al and ^{29}Si calculated errors of the NMR parameters derived from the simulation of the 2D D-HMQC experiment performed on Al1−SiO_{2-500} and Al10−SiO_{2-500}.

site	%	$\bar{\delta}_{iso}$ (ppm)	$\Delta\delta_{iso}$ (ppm)	$\bar{C}_Q$ (MHz)
Al1−SiO_{2-500}				
$^{[4]}Al_{(1Si)}$	2.7	0.7	1.41	0.46
$^{[4]}Al_{(3Si)}$	4.4	0.3	1.11	0.26
$^{[5]}Al_{(1Si)}$		0.3	0.99	0.23
$^{[6]}Al_{(1)}$	0.4	1.9	3.56	0.92
$^{[6]}Al_{(2)}$	0.8	0.2	1.16	0.52
$Q^3_{(1Al)}$		1.1	1.14	
$Q^4_{(1Al)}$		0.3	0.40	
Al10−SiO_{2-500}				
$^{[4]}Al_{(1Si)}$	1.3	0.2	0.19	0.24
$^{[4]}Al_{(3Si)}$	2.4	0.3	0.90	0.25
$^{[5]}Al_{(1Si)}$		0.2	0.83	0.22
$^{[6]}Al_{(1)}$	0.3	0.1	2.34	0.18
$^{[6]}Al_{(2)}$	0.9	0.9	2.37	0.80
$Q^3_{(2Al)}$		0.6	0.74	
$Q^4_{(1Al)}$		0.3	0.38	

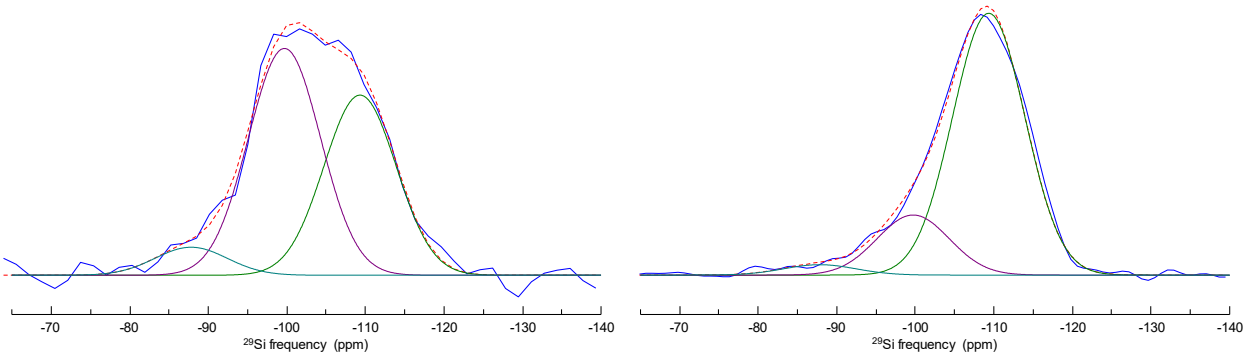

Figure S11. ^{29}Si CPMG-detected MAS experiments performed on Al10-SiO_{2-500} at 7.0 T: ^{29}Si{^{1}H} CPMAS (left) and direct ^{29}Si (right) spectra. Experimental (blue), simulation (dashed red) and individual Gaussian components (colored).

Table S8. NMR parameters derived from the simulation of the ^{29}Si{^{1}H} CPMG experiments on Al10−SiO_{2-500} using Gaussian lines with identical widths.

Site	%direct	%CPMAS	Position (ppm)	Width (ppm)
$Q^{[4]}$	78.6	41.5	−109.3	10.8
$Q^{[3]}$	18.2	52.1	−99.7	10.8
$Q^{[2]}$	3.2	6.4	−87.8	10.8

Table S9. Correlation map of the 2D $^{27}Al\{^{29}Si\}$ D-HMQC experiments performed on Al1−SiO_{2-500} and Al10−SiO_{2-500}. Values are percentages of each individual 2D component with related errors given in parenthesis.

Al1−SiO_{2-500}						Al10−SiO_{2-500}					
	$^{[4]}Al_{(3Si)}$	$^{[4]}Al_{(4Si)}$	$^{[5]}Al_{(2Si)}$	$^{[6]}Al_{(1)}$	$^{[6]}Al_{(2)}$		$^{[4]}Al_{(2Si)}$	$^{[4]}Al_{(3Si)}$	$^{[5]}Al_{(2Si)}$	$^{[6]}Al_{(1)}$	$^{[6]}Al_{(2)}$
$Q^4_{(1Al)}$		32.1 (4.4)	27.4 (4.1)		2.6 (0.8)	$Q^4_{(1Al)}$		33.3 (2.4)	19.1 (1.3)		3.4 (0.9)
$Q^3_{(1Al)}$	18.6 (2.7)		17.5 (2.3)	1.8 (0.4)		$Q^3_{(2Al)}$	22.7 (1.3)		20.3 (1.5)	1.3 (0.3)	

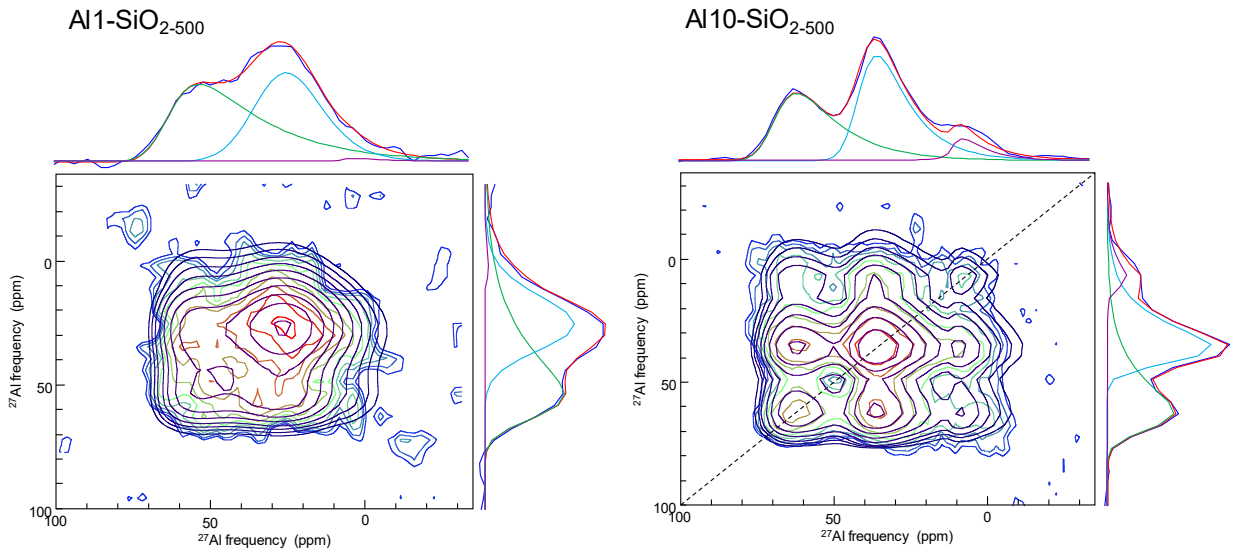

Figure S12. ^{27}Al DQ/SQ $R2_1^2$MAS NMR correlation 2D experiments for Al1−SiO_{2-500} (left) and Al10−SiO_{2-500} (right) with projections along each dimension. Simulation of the 2D data are given in grey and individual components are given in the projections in color with their sum in red.

Table S10 ^{27}Al NMR parameters derived from the simulation of the ^{27}Al/^{27}Al DQ/SQ dipolar-based correlation experiment. (*) Lorentzian broadening. Correlation map of the 2D ^{27}Al{^{29}Si} D-HMQC experiment performed on Al1−SiO_{2-500} and Al10−SiO_{2-500}. Values are percentages of each individual 2D component. All related errors are given in parenthesis.

site	$\bar{\delta}_{iso}$ (ppm)	$\Delta\delta_{iso}$ (ppm)	$\bar{C}_Q$ (MHz)	$\bar{\delta}_{iso}$ (ppm)	$\Delta\delta_{iso}$ (ppm)	$\bar{C}_Q$ (MHz)
$^{[4]}$Al	65.7 (0.3)	13.2 (0.8)	13.5 (0.5)	70.6 (0.2)	10.6 (0.4)	10.8 (0.3)
$^{[5]}$Al	32.9 (0.7)	21.4 (0.9)	7.93 (0.5)	42.8 (0.1)	9.63 (0.3)	9.30 (0.1)
$^{[6]}$Al	7.8 (9.5)	2.3* (18.0)	8.40 (11.4)	11.8 (0.4)	3.16* (1.4)	7.48 (0.4)
	$^{[4]}$Al	$^{[5]}$Al	$^{[6]}$Al	$^{[4]}$Al	$^{[5]}$Al	$^{[6]}$Al
$^{[4]}$Al						4.0 (0.8)
$^{[5]}$Al		67.3 (5.3)			43.2 (1.5)	6.7 (0.6)
$^{[6]}$Al	12.6 (1.4)	19.2 (0.6)	1.0 (1.1)	16.1 (0.9)	24.0 (0.4)	6.0 (0.5)

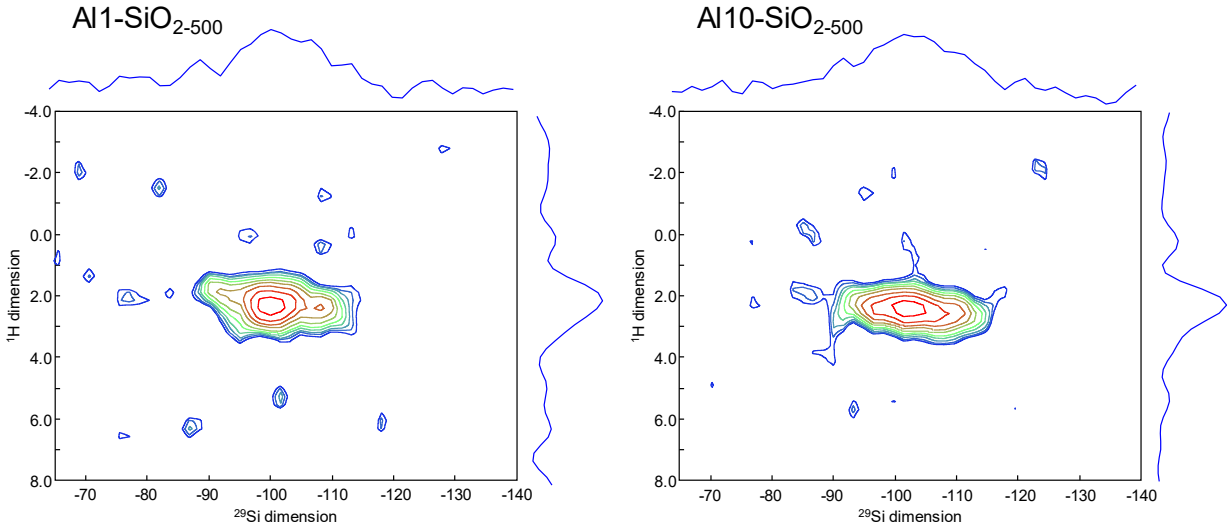

Figure S13. ^{29}Si{^{1}H} VACP CPMG-detected MAS experiments performed on Al1−SiO_{2-500} (left) and Al10−SiO_{2-500} (right) at 7.0 T using a contact time of 0.5 ms and acquiring 512 echos with an inter-pulse delay of 8 ms.

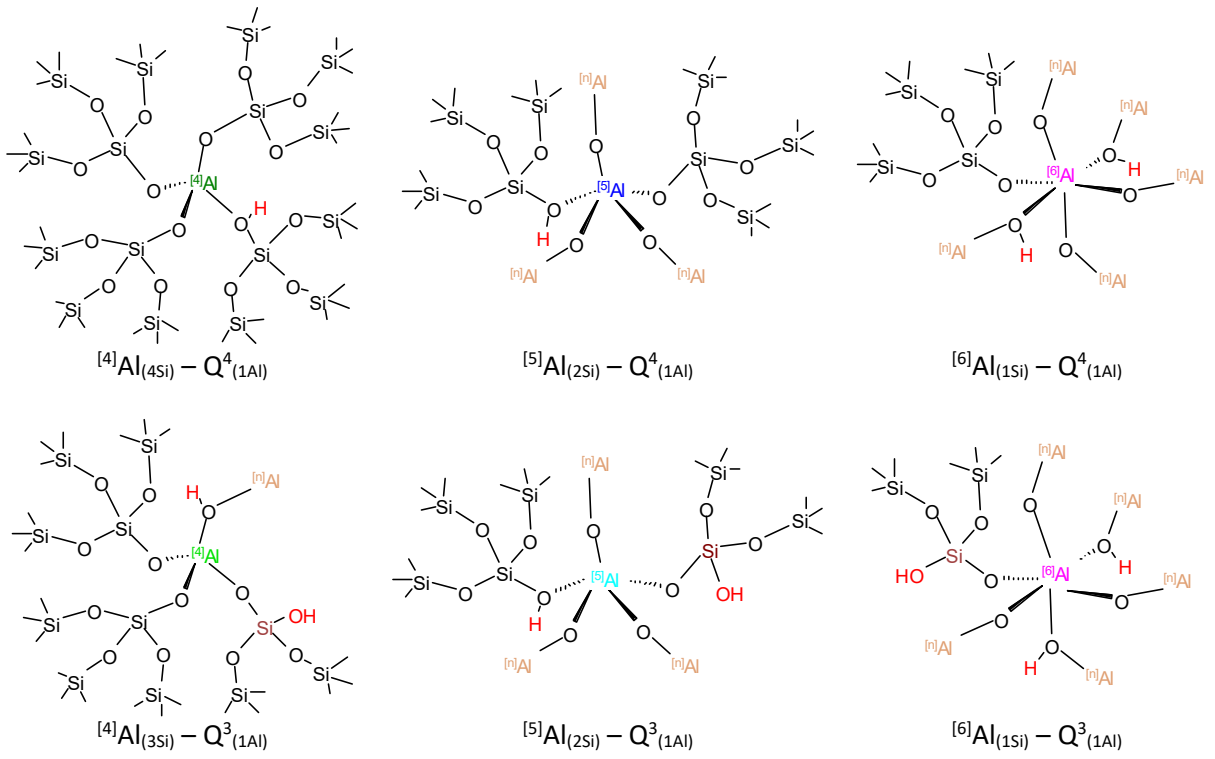

Figure S14. Sketch of the most probable aluminum environments in the Al1−SiO_{2-500} material according to experimental evidences of this study.

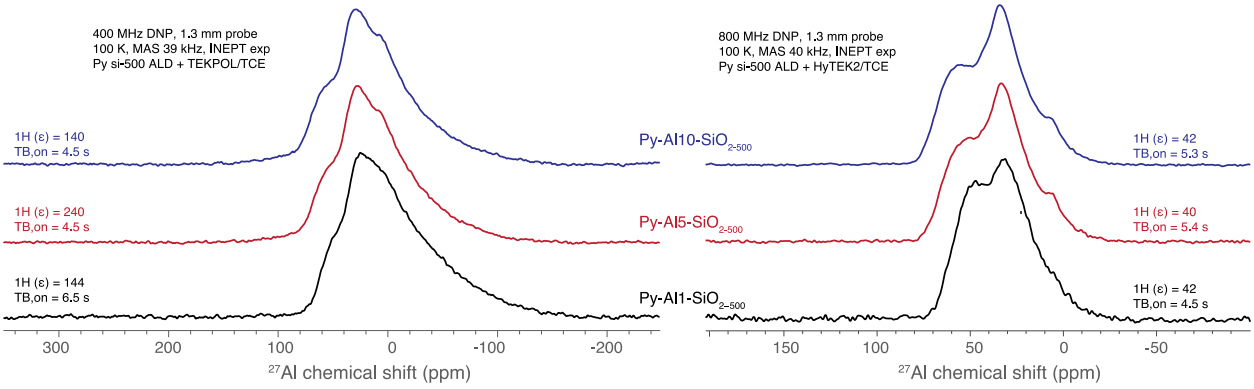

Figure S15. $^{27}Al\{^{1}H\}$ D-R-INEPT DNP NMR spectra of Py-Al1−SiO_{2-500} (black), Py-Al5−SiO_{2-500} (red), and Py-Al10−SiO_{2-500} (blue) recorded at 9.4 and 18.8 T using a 1.3 mm probe, operated at 100 K, and irradiation of suitable microwave powers for the respective biradical used. Corresponding ^{1}H DNP enhancements and DNP build-up times ($T_{B,on}$) are reported.

Table S11 ^{15}N NMR parameters derived from the simulation of the ^{15}N DNP enhanced NMR spectra of Py-Al1−SiO_{2-500}, Py-Al5−SiO_{2-500}, and Py-Al10−SiO_{2-500}. Values are percentages of each individual 2D component. All related errors are given in parenthesis.

	Py-Al1−SiO_{2-500}		Py-Al5−SiO_{2-500}		Py-Al10−SiO_{2-500}	
site	$\bar{\delta}_{iso}$ (ppm)	$\Delta\delta_{iso}$ (ppm)	$\bar{\delta}_{iso}$ (ppm)	$\Delta\delta_{iso}$ (ppm)	$\bar{\delta}_{iso}$ (ppm)	$\Delta\delta_{iso}$ (ppm)
Py-$L_{(1)}$	260.2(0.29)	20.3 (0.62)	260.4 (0.03)	15.0 (0.05)	262.1 (0.05)	14.5 (0.09)
Py-$L_{(2)}$	239.1 (0.13)	15.3 (0.34)	239.8 (0.03)	21.3 (0.12)	242.6 (0.08)	24.3 (0.19)
Py-$H^+_{(1)}$	208.1 (0.40)	20.3 (0.46)	209.2 (0.12)	19.3 (0.12)	216.2 (0.30)	9.5 (0.58)
Py-$H^+_{(2)}$	203.8 (0.10)	11.8 (0.33)	203.7 (0.04)	10.5 (0.13)	204.5 (0.15)	13.3 (0.28)

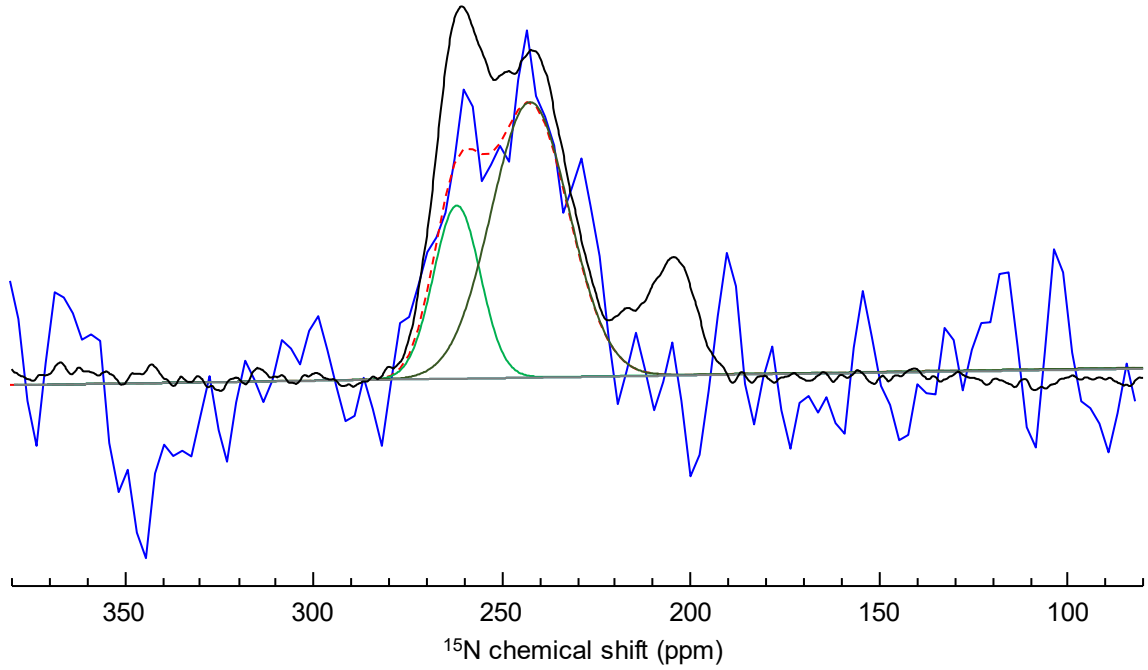

Figure S16. One-dimensional ^{15}N DNP SENS spectra of Py-Al10−SiO_{2-500} recorded via ^{15}N{^{27}Al} J-HMQC (blue) and ^{1}H-^{15}N CP (black) experiments. Under 10 KHz MAS using Bruker DNP spectrometer at 9.4 T equipped with a 1.3 mm probe, operated at 100 K, and irradiation of suitable microwave powers for the respective biradical used. Deconvolution uses positions and width of components listed in Table S11 for Py-Al10−SiO_{2-500}.

References

1. Brunauer, S.; Emmett, P. H.; Teller, E., Adsorption of Gases in Multimolecular Layers. *J. Am. Chem. Soc.* **1938,** *60*, 309-319.
2. Miikkulainen, V.; Leskelä, M.; Ritala, M.; Puurunen, R. L., Crystallinity of Inorganic Films Grown by Atomic Layer Deposition: Overview and General Trends. *J. Appl. Phys.* **2013,** *113*, 021301.
3. Giovine, R.; Trébosc, J.; Pourpoint, F.; Lafon, O.; Amoureux, J.-P., Magnetization Transfer from Protons to Quadrupolar Nuclei in Solid-State NMR using PRESTO or Dipolar-Mediated Refocused INEPT Methods. *J. Magn. Reson.* **2019,** *299*, 109-123.